Electronic Supplementary Information (ESI)

Degassed micromolding lithography for rapid fabrication of anisotropic hydrogel microparticles with high-resolution and high uniformity

Hyeon Ung Kim, Yong Jun Lim, Hyun Jee Lee, Nak jun Lee, and Ki Wan Bong*

Department of Chemical and Biological Engineering, Korea University, Seoul 02841, Republic of Korea. E-mail: bong98@korea.ac.kr, TEL: +82 02 3290 3294

1. Supplementary Notes

1.1 Mathematical model of liquid loading into the degassed mold.

We determined the air flux on the surface of the degassed PDMS block, $N_{air}(t)$, using the computational method (COMSOL) with the following parameters, where the initial air concentration in PDMS is 0.489 mol m^{-3}, the boundary condition is 4.89 mol m^{-3}, the diffusivity of air is 3.4*10^{-9} m^2 s^{-1}, the thickness of the block is 3 mm and the bottom surface of the PDMS is blocked with glass. $N_{air}(t)$ is given by

$$N_{air}(t) = a * \ t^b \ [\frac{mol}{m^2 sec}] \tag{1}$$

Where *a* is 0.0001 and *b* is -0.441, and t is larger than 20 because it takes about 20 sec for the addition of the liquid after removing the micromold from the vacuum chamber.
In our liquid loading model, we estimate that capillary pressure (P_c) and pressure drop (ΔP) will be balanced after the induction time has elapsed. Therefore, ΔP for the square cross-section is calculated as

$$\Delta P \ = P_c = \frac{2\gamma \cos\theta}{\frac{W_0}{2}} = 1{,}156 \ Pa \tag{2}$$

$$P_i = P_0 - \ \Delta P = 100{,}169 \ Pa \tag{3}$$

Where γ is 0.0728 N/m, θ is 113.4°, P_0 is 101,325 Pa, and W_0 is 100 μm.
As the ratio of pressure change ($\frac{P_i}{P_0} * 100\ (\%)$) becomes smaller than 1.2%, we estimate the molar volume of the trapped air between the liquid and the micromold to be constant at 0.0224 m^3 mol^{-1}. Therefore, $N_{air}*$ surface area of micromold can be converted to the volumetric air uptake rate in the micromold. The volume of the loaded liquid can be calculated as follow,

$$\big(H_0 - H(t)\big) * {W_0}^2 = \frac{22.4}{1{,}000} * \int_{20}^{20+t} N_{air}(x) * ({W_0}^2 + 4W_0 H(x))dx \tag{4}$$

Where H_0 is the height of the micromold, $H(t)$ is the height of entrapped air bubble which is H_0 at t= 20 sec, W_0 is the width of the rectangular-shape micromold. When equation (4) is differentiated,

$$-\frac{W_0}{W_0 + 4H} dH = \frac{22.4}{1{,}000} * a * \ (t+20)^b dt \tag{5}$$

and integrating between the limits indicated, we can obtain

$$-\int_{H_0}^{0} \frac{W_0}{W_0 + 4H} dH = \frac{22.4}{1{,}000} \int_0^{t_D} a * \ (t+20)^b dt \tag{6}$$

From equation (6), liquid loading time (t_D) can be calculated in a micromold of specific geometry as below,

$$\frac{W_0}{4} \ln \frac{W_0 + 4H_0}{W_0} = \frac{22.4 \quad a}{1{,}000 b + 1} \left[(20 + t_D)^{b+1} - 20^{b+1}\right] \tag{7}$$

When $W_0 = 100\ \mu m$, $H_0 = 25\ \mu m$, t_D was calculated to be 57.8 sec with a percentage error of 1.9% where the experimental t_D was 56.7 sec. For this calculation, liquid properties are not considered (e.g., wettability and viscosity). The effect of liquid properties in DML is explained in Supplementary Notes 1.2 and 1.3.

1.2 Effect of surface tension in liquid loading.

From equation 2, P_c value of water can be calculated as

$$\Delta P \ = P_c = \frac{2\gamma \cos\theta}{\frac{W_0}{2}} = 1{,}156 \ Pa \tag{2}$$

Where W_0 is 100 μm, γ is 0.0728 N m^{-1} and θ is 113.4°. Among the commonly available liquids, water has a high surface tension. Therefore, the largest P_c value can be estimated to 2,660 Pa, where γ is 0.0728 N m^{-1} and θ is 180°. The larger the $P_c\ value$, the

greater the force will be required to deform the air-liquid interface, which induces to decrease the air uptake rate of the degassed mold.

In Supplementary Notes 1.1, we calculated $N_{air}(t)$ without considering the P_c value. By changing the boundary condition from 4.89 mol m^{-3} to 4.7616 mol m^{-3}, air flux of the degassed PDMS block after considering the capillary pressure, $N_{air}'(t)$, can be simulated as follow

$$N_{air}'(t) = a * t^b \left[\frac{mol}{m^2 sec}\right] \tag{8}$$

Where *a* is 0.0001 and *b* is -0.484.

Modified t_D is found to be 65.94 sec after applying $N_{air}'(t)$ in equation 7. The difference in the t_D by the capillary pressure was 12.3%, which confirmed that the t_D of the degassed micromold is not significantly affected by wettability of the liquid.

1.3 Effect of viscosity in liquid loading.

In previous study, the viscosity of the liquid can be distinguished by their flow rate in a degassed PDMS pump system.[1] However, t_D is not significantly affected by the viscosity of liquid in a degassed micromold (Fig. S1). We suggest that this difference is due to the characteristic length of the channel, the volume divided by the cross-sectional area, which is normally larger than 10^4 in a microfluidic channel but, in the case of a micromold, the characteristic length is 25. When the characteristic length is large, void volume of the channel is not significantly changed by the volume occupied by the liquid. Therefore, $P_i(t)$ by the vacuum pumping of the PDMS will be maintained at a specific value regardless of the viscosity of the liquid. On the contrary, we estimated that ΔP profile in the micromold is affected by viscosity of the liquid.

After the induction time, a low-viscosity liquid flows with the same rate as the air uptaken by the PDMS similar to the isobaric compression of a piston, so that $P_i(t)$ is converged at P^*. Whereas, the flow rate of a high-viscosity liquid is less than the air uptake rate by the PDMS, thus $P_i(t)$ is decreased to P_{low}, which is smaller than P^*. Therefore, according to our assumption, viscous flow resistance is partially compensated by the change in ΔP.

1.4 Calculation of induction time.

To calculate the induction time with simple relation, we estimate that $N_{air}(t)$ is not a function of the pressure of the trapped air. Therefore, ΔP comes from air uptake of degassed PDMS is calculated as follow,

$$\Delta P = \frac{\Delta nRT}{V}\,[Pa] \tag{9}$$

$$\Delta n = \int_{20}^{20+t} N_{air}(x) * ({W_0}^2 + 4W_0H_0)dx \tag{10}$$

Where *R* is the ideal gas constant, *T* is the Kelvin temperature, and *V* is the volume of the micromold.

In our liquid loading model, ΔP and P_c are balanced at the induction time. Therefore, the induction time can be calculated by integrating equation 2 and 9 as below,

$$\frac{2\gamma\cos\theta}{\frac{W_0}{2}} = \frac{\int_{20}^{20+t} a * t^b * ({W_0}^2 + 4W_0H_0)dxRT}{V} \tag{11}$$

When γ is 0.0728 N m^{-1}, θ is 113.4°, W_0 is 100 μm, H_0 is 25 μm, *a* is 0.0001, *b* is -0.441, *R* is 8.314 m^3 Pa $K^{-1}mol^{-1}$ and *T* is 298 K, the induction time can be deduced as 0.22 sec.

1.5 Measurement of residual layer.

In order to make a film in the condition with minimal oxygen inhibition, the mold block with the precursor was placed in the vacuum chamber. With the vacuum pump was in operation, nitrogen gas was pumped in for 5 minutes to purge the oxygen inside the chamber. Thereafter, UV (100 mW cm^{-2}) was applied for 10 minutes. Fully cured polymer film was cutted for the measurement of the thickness of the wet precursor layer between the mold block and the cover.

1.6 Estimation of minimum height of the mold to fabricate separated particles

The polymerization is known to be initiated from the center of the microchannel.[2] Therefore, in DML, particle is synthesized from the center between the top of the mold and the bottom of the residual layer. When the height of the mold is lower than the thickness of residual layer, polymer film can be formed rather than individual particles because the growth of the polymer is contained in the residual

layer. To estimate minimum height of the mold to fabricate separated particles, we introduced rule of thumb where the particles are fabricated if $\frac{H_M + H_R}{2}$ is larger than $2H_R$ where H_M is the height of the mold and H_R is the thickness of the residual layer. The minimum H_M that satisfies the assumption is 6.6 μm.

2. Supplementary Figures

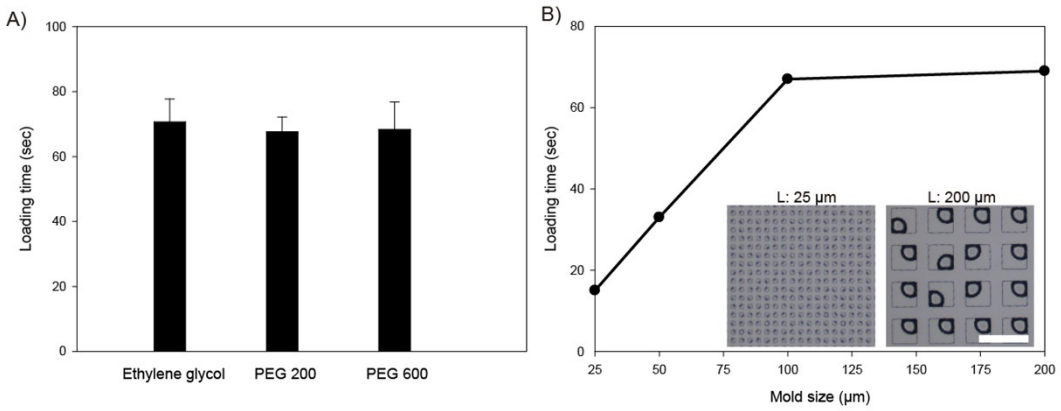

Fig. S1 Liquids loading time in various conditions. A) The loading time of using liquids with varying viscosity (Ethylene glycol, PEG 200 and PEG 600). Each bar represents the mean value from three independent experiments. Error bars represent the standard deviation. B) The loading time of liquid into micromolds of varying cross-section width but a constant height (height : 25 μm). Scale bar = 400 μm.

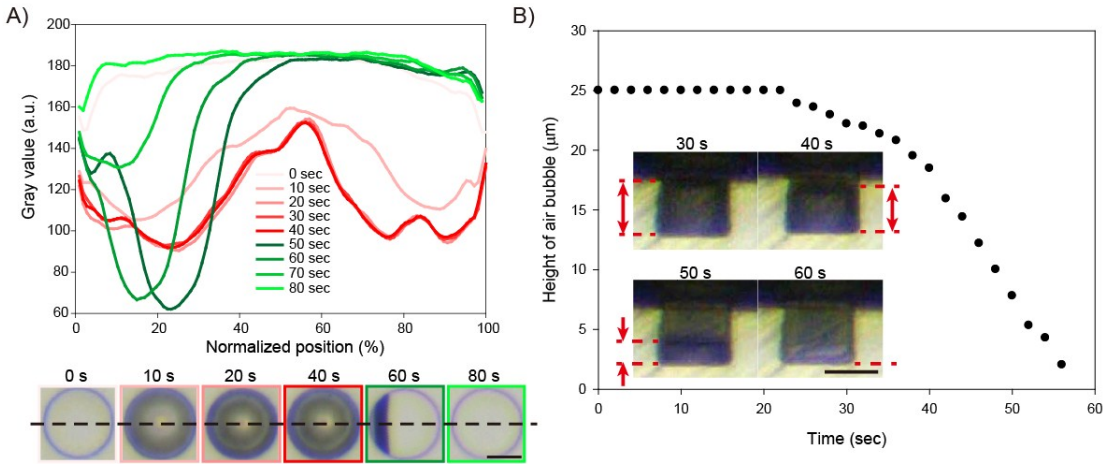

Fig. S2 The parameters of liquid loading in a degassed micromold. A) Gray value profiles (a.u. = arbitrary units) taken across the region of the micromold shown in below. As the induction time is too short to be observed in fully degassed micromold, the mold template was partially degassed (3 min). B) The height of the air-bubble interface as a function of time. The degassing time of the micromold was 60 min. In order to observe the sides of the micromold, it was sliced and mounted on the microscope at a 90° angle. Scale bars = 50 μm.

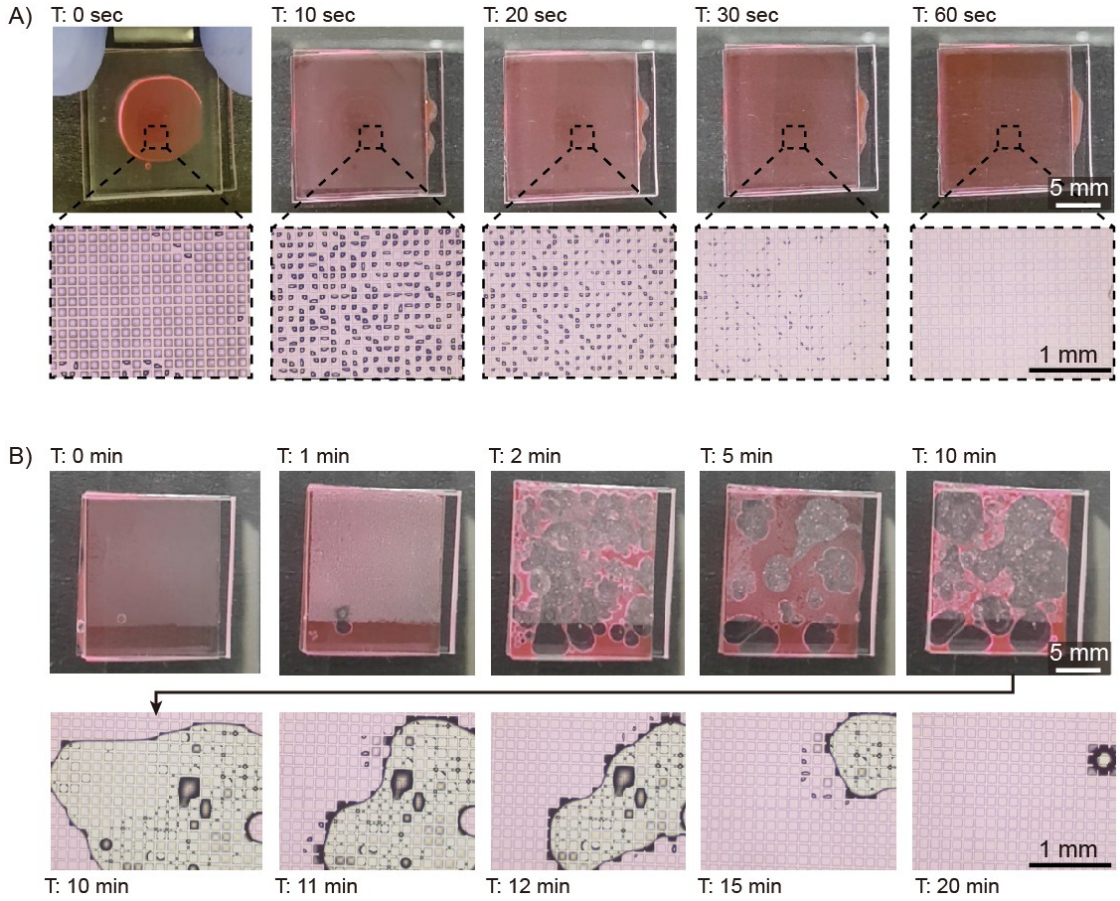

Fig. S3 Time-lapse images of the precursor loading. A) The sequence of precursor loading into micromolds degassed for 60 mins. Macroscopic images (top) and microscopic images (bottom) taken from a mounted camera. B) The sequence of precursor loading with vacuum casting. After taking macroscopic images (top) in vacuum chamber (0.1 atm), the mold was taken out and observed under the microscope (bottom).

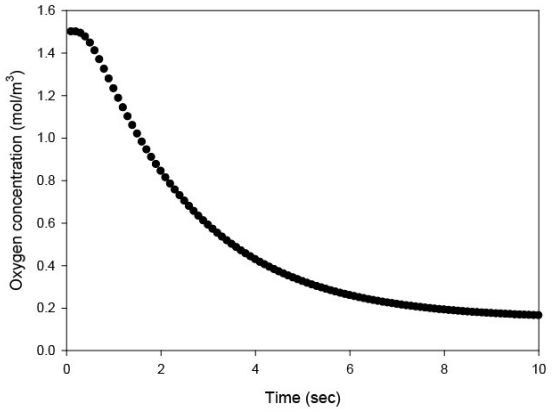

Fig. S4 The change in oxygen concentration in the precursor with time in the degassed micromold. The following parameters were used for the calculation of the oxygen concentration, the dimensions of the precursor: 25*100*100 μm^3; the initial oxygen concentration: 1.5 mol m^{-3}; the boundary condition: 0.15 mol m^{-3}; the diffusivity: $2.84*10^{-11}$ m^2 s^{-1}. The oxygen concentration was calculated at the center point in the 3D space of the precursor using the finite element method in COMSOL software.

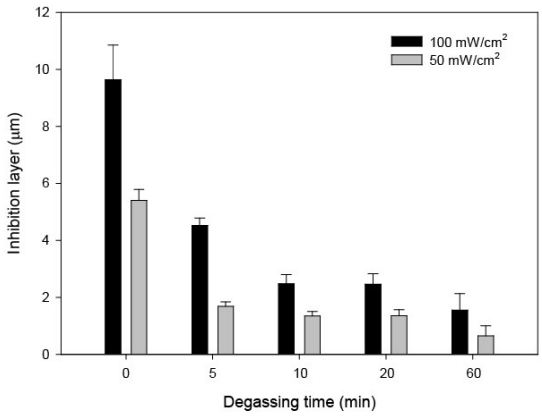

Fig. S5 Oxygen inhibition layer verses degassing time. Each micromold size is 25*100*100 μm^3 and 1 sec of UV was exposed. Each point represents mean value from 10 particles. Error bars represent standard deviation.

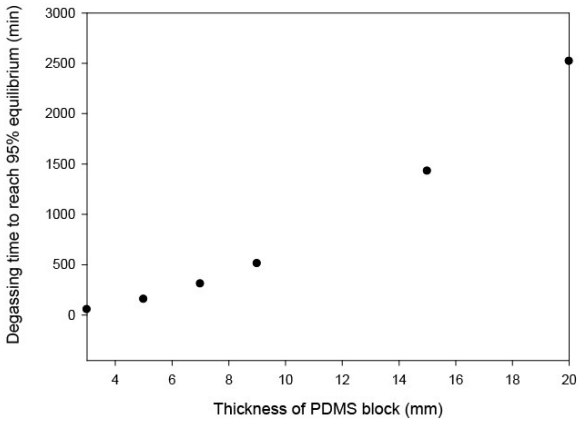

Fig. S6 Degassing time needed to reach 95% equilibrium oxygen concentration in the vacuum chamber (0.1 atm) for PDMS blocks with varying thickness. With assumption that oxygen can only diffuse through the top surface of the PDMS blocks, we calculated the time to reach 95% equilibrium oxygen concentration at the bottom surface using the finite element method in COMSOL software. The following parameters were used for the calculation, the initial oxygen concentration in the PDMS: 1.5 mol m^{-3}; the equilibrium oxygen concentration in the PDMS: 0.15 mol m^{-3}; the diffusivity: $2.84*10^{-11}$ m^2 s^{-1}.

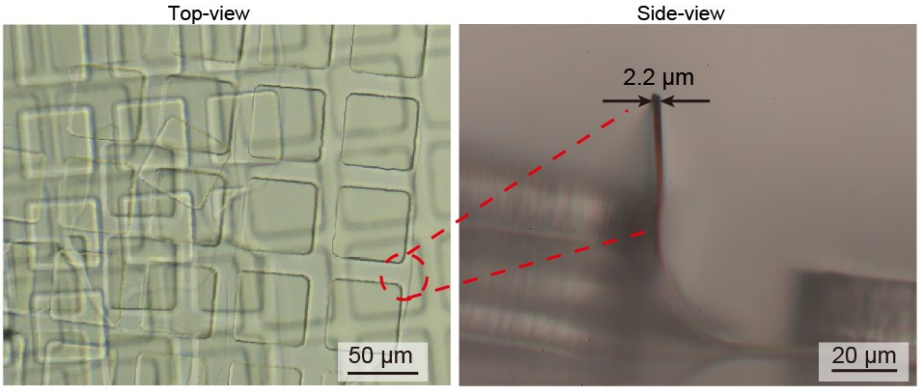

Fig. S7 Thickness of the residual precursor layer. Detailed information on the curing experiment is described in Supplementrary Notes.

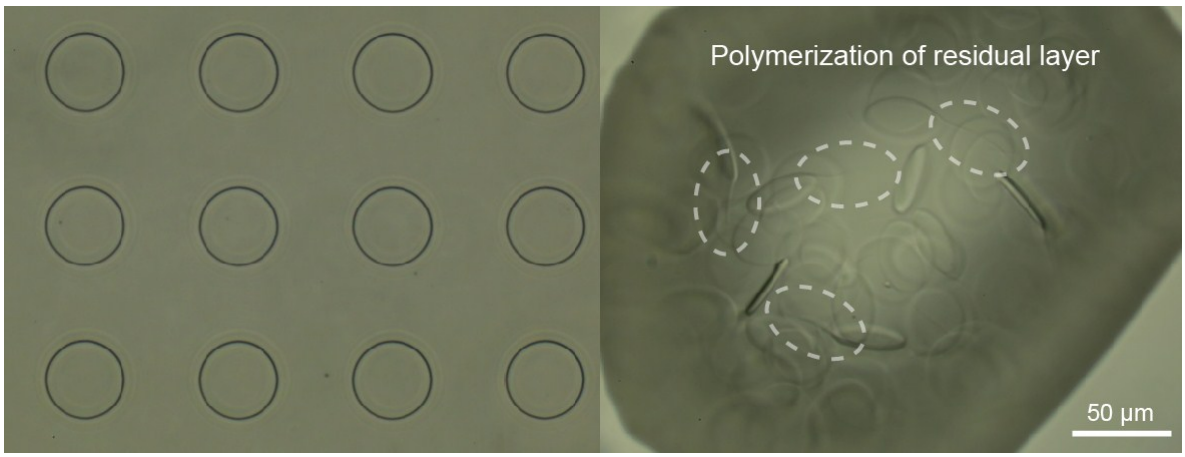

Fig. S8 Particle fabrication at 5 μm micromold height .

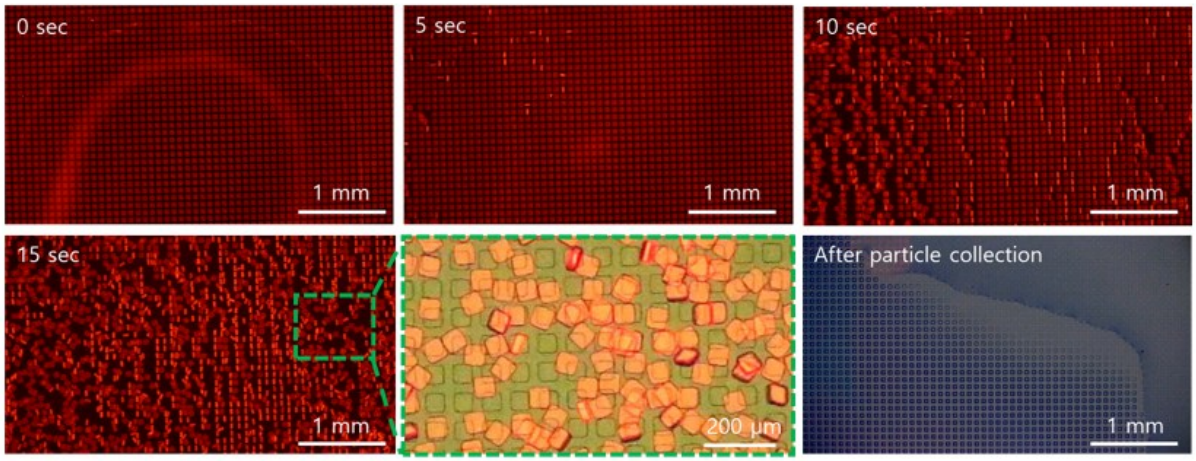

Fig. S9 Time-lapse micrograph of the particles in recovery solution.

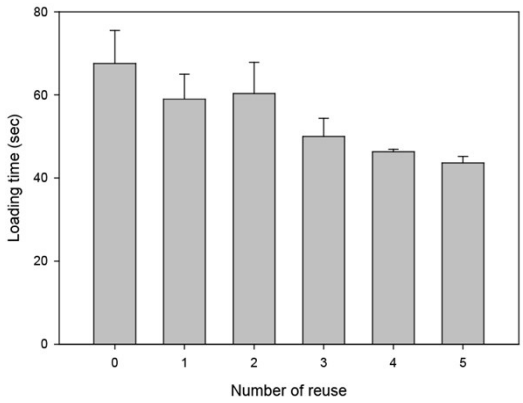

Fig. S10 Comparison of precursor loading times with sequential reuse of the mold templates.

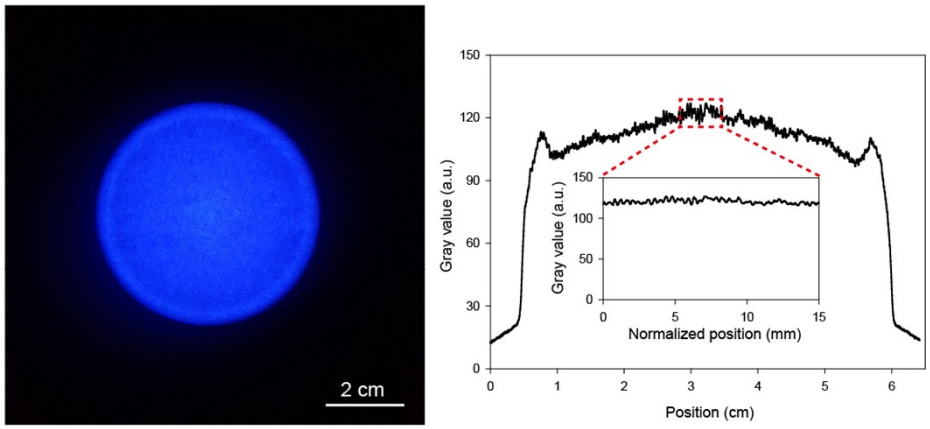

Fig. S11 The profile of UV intensity of a UV-LED lamp. Macroscopic image of a UV-LED lamp (left). The gray value profile given by the corresponding UV-LED lamp is shown (right).

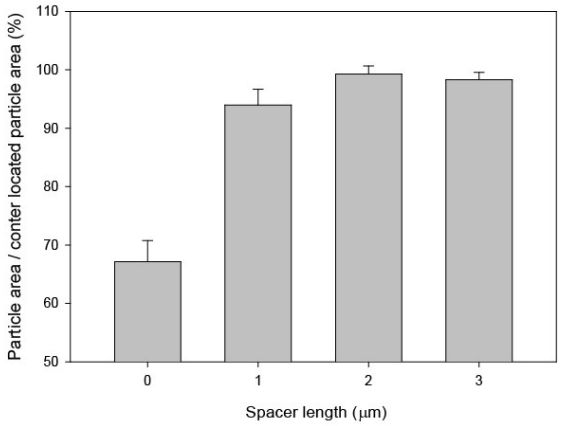

Fig. S12 Optimization of the spacer length. The area of the particles synthesized in micromolds resided at the edge of the mold template was divided by the area of those located at the center of the template. UV irradiation (100 mW cm^{-2}, 1 sec) was applied to each 25*50*50 μm^3 rectangular micromold. Each point represents the mean value from 10 particles. Error bars represent the standard deviation.

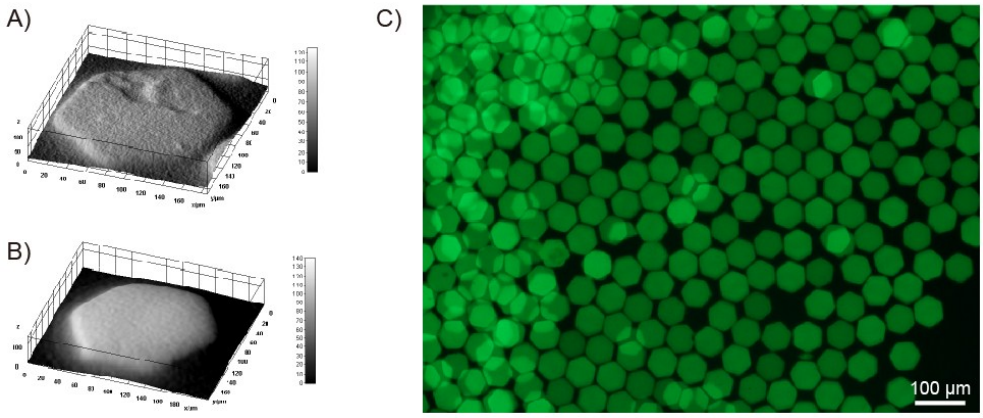

Fig. S13 The synthesis of protein encapsulated hydrogel microparticle. A) & B) The 3D surface plots of protein encapsulated hydrogel microparticles are shown, A) a particle synthesized in a non-degassed micromold with precursor loaded by scrubbing with a pipette for 120 sec, B) a particle synthesized by DML method. C) Fluorescent image of a large-scale synthesis of protein encapsulated hydrogel particles using DML method.

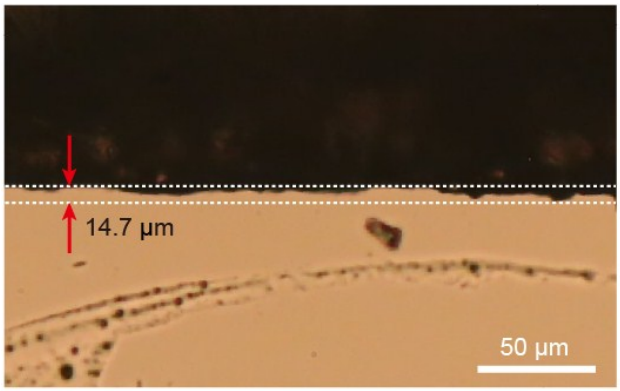

Fig. S14 The surface of a 3D-printed master.

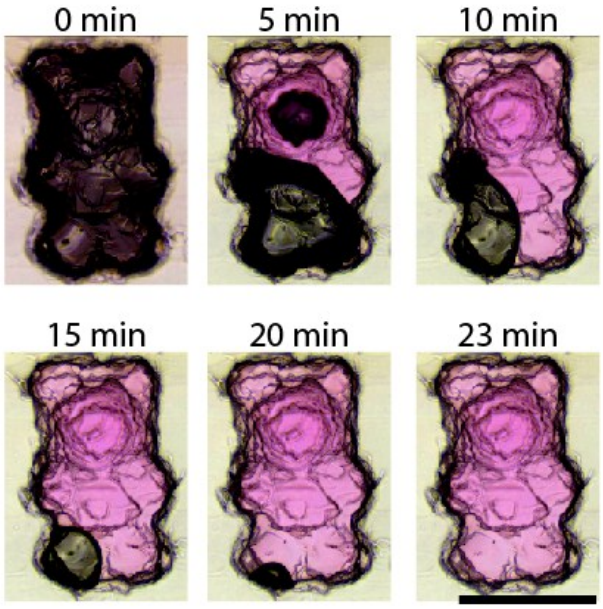

Fig. S15 Time-lapse micrographs of degassed 3D micromold filled with PEG-DA precursor. Scale bar = 1mm.

Table S1. Calculated air flux rate and precursor loading time according to diffusivity.

Diffusivity ($10^{-9}m^2/s$)	$N_{air}(t) = a * t^b [\frac{mol}{m^2 sec}]$		Liquid loading time (sec) (W_0:100μm, H_0:25μm)
	a	b	
34	0.0005	-0.522	28.1
3.4 [PDMS][3]	0.0001	-0.441	57.8
0.34	0.00004	-0.463	162.3
0.034	$8*10^{-7}$	-0.069	1519.5

Table S2. Quantitative comparison of productivity between DML and microfluidic synthesis techniques. Estimated automation setup is calculated as the radius and width of the mold roller is 30 cm and 100 cm and roller speed is 1.2 feet / min which is 10% of rolling speed of previously developed roll-to-roll particle fabrication system.[4]

	Illumination area	Process time	Productivity (particles: 100*100μm^2)	Reference
Stop Flow lithography	0.5mm*0.5mm	~0.36sec/cycle	~9*10^4 particles/hour	5
Optofluidic maskless lithography	-	40 μm/sec	~6*10^4 particles/hour	6
Contact flow lithography	16mm*10mm	~7.5sec/cycle	~6*10^6 particles /hour	7
DML	10cm*10cm	~120 sec	~9*10^6 particle/hour	Manual setup
	-	~1.2 feet / min	~10^9 particle/hour	Estimated automation setup

Movie S1. The movie is an actual-time video of the precursor loading in degassed micromold (100*100*25 μm3).

Movie S2. The movie is an actual-time video of particle harvest from the mold (50*50*25 μm^3).

References

1 X. Tang, B. Zheng, *Analyst,* 2011, ***136***, 1222-1226.
2 D. Dendukuri, P. Panda, R. Haghgooie, J.M. Kim, T.A. Hatton, P.S. Doyle, *Macromolecules*, 2008, ***41***, 8547-8556.
3 L.F. Xu, H. Lee, D. Jetta, K.W. Oh, *Lab Chip,* 2015, ***15***, 3962-3979.
4 C.H. Kapadia, S. Tian, J.L. Perry, J.C. Luft, J.M. DeSimone, *Mol. Pharm.*, 2016, ***13***, 3381-3394.
5 D. Dendukuri, S.S. Gu, D.C. Pregibon, T.A. Hatton, P.S. Doyle, *Lab Chip*, 2007, ***7***, 818-828.
6 S.E. Chung, W. Park, H. Park, K. Yu, N. Park, S. Kwon, *Appl. Phys. Lett.*, 2007, ***91***, 041106.
7 G.C. Le Goff, J. Lee, A. Gupta, W.A. Hill, P.S. Doyle, *Adv. Sci.*, 2015, ***2***, 1500149.